Chapter 4: Enhancement in modulus of elasticity by TiC reinforcement in austenitic low-density steel

4.1 Introduction

An austenitic low-density steel with TiC reinforcement (P2) (Fe-18Mn-6.5Al-1.25C-2.5Ti) is produced using vacuum induction melting, followed by hot rolling (1050 °C, 1 h, 75% reduction in thickness) and solution treatment (950 °C, 30 min, Water quenched) (PD2-S). Microstructure and mechanical properties are reported in Chapter 4. Presence of TiC decreases the grain size, increases strength and modulus of elasticity.

4.2 Results

4.2.1 Phase fraction Diagram

The calculated phase fraction diagram of PD2, obtained using ThermoCalc software (Figure 4.1) quantitatively represents the volume fraction of each phase as a function of temperature. At a temperature of 1080°C, the austenite phase constitutes 94.2% of the volume, while the TiC phase (FCC_A12) accounts for 4.8% along with 1 % of delta ferrite. Beyond 1073°C, the emergence of the BCC_A2 phase is observed. The homogenization temperature is selected as 1080°C, given the absence of TiC dissolution across the entire temperature spectrum. In the temperature interval of 630°C to 1073°C, an austenite and TiC coexist, with negligible variation in their respective volume fractions.

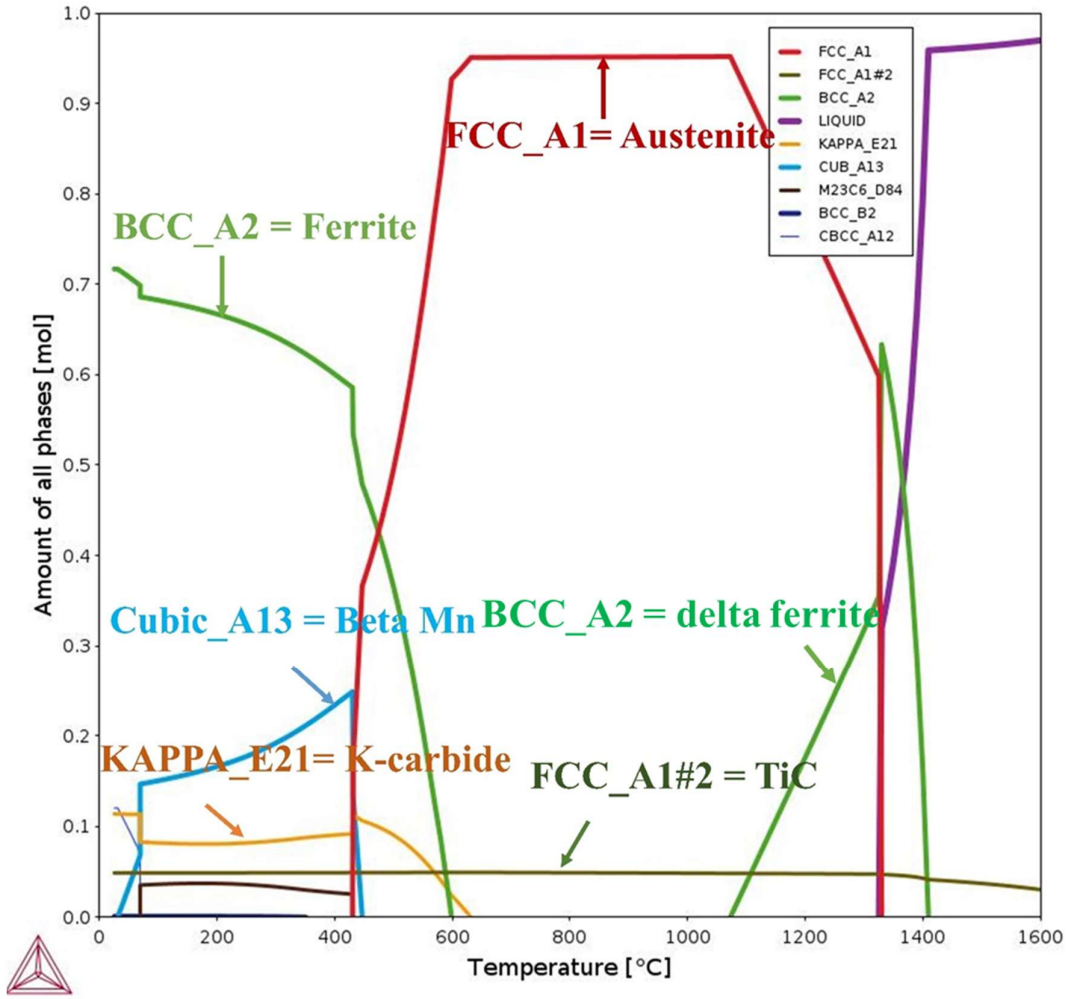

Figure 4.1: Phase fraction diagram of PD2 with the amount of all phases with respect to temperature.

4.2.2 Physical Properties

The density of PD2-S, as determined using Archimedes' principle, together with the values of the elastic modulus, shear modulus, and Poisson's ratios obtained through ultrasonic testing are presented in Table 4.1. The density of PD2-S is 6.84 ± 0.04 g/cc. The elastic modulus, shear modulus, and Poisson ratio values for PD2-S are 176 ± 0.43 GPa, 70 GPa, and 0.26, respectively.

Table 4.1: Density, Elastic modulus, Shear modulus, and Poisson ratio of PD2-S.

Steel	Density (g/cc)	Longitudinal velocity (m/s)	Transverse velocity (m/s)	Poisson ratio	Shear modulus (GPa)	Elastic modulus (GPa)
PD2-S	6.84± 0.04	5593 ± 16.8	3201 ± 61	0.26	70.0	176± 0.43

4.2.3 Microstructural Characterization

The optical micrograph of PD2-S (Figure 4.2 (a)) shows austenite grains with a size of 10 ± 3 μm, along with TiC particles predominantly rectangular in shape. A small amount of delta ferrite is also observed in PD2-S. The x-ray diffraction pattern of PD2-S (Figure 4.2 (b)) reveals the presence of 92.5% austenite, along with 3% delta ferrite and 4.5% TiC particles. The scanning electron micrograph (SEM) of PD2-S (Figure 4.2 (c)) displays the presence of TiC and corresponding Energy Dispersive Spectrum (EDS) (Figure 4.2(e)) conforms the indicated particle to be TiC. The SEM secondary electron image (Figure 4.2 (d)) of PD2-S describes the uniform spatial distribution of TiC particles inside the PD2-S. Another higher resolution SEM secondary electron micrograph of PD2-S is taken to measure size of TiC particles (Figure 4.2(f)). All individual particles are measured with the help of ImageJ software. A size distribution chart is given in Figure 4.2 (g). The average size of the TiC particles is 2.59 μm with standard deviation of 1.6 μm.

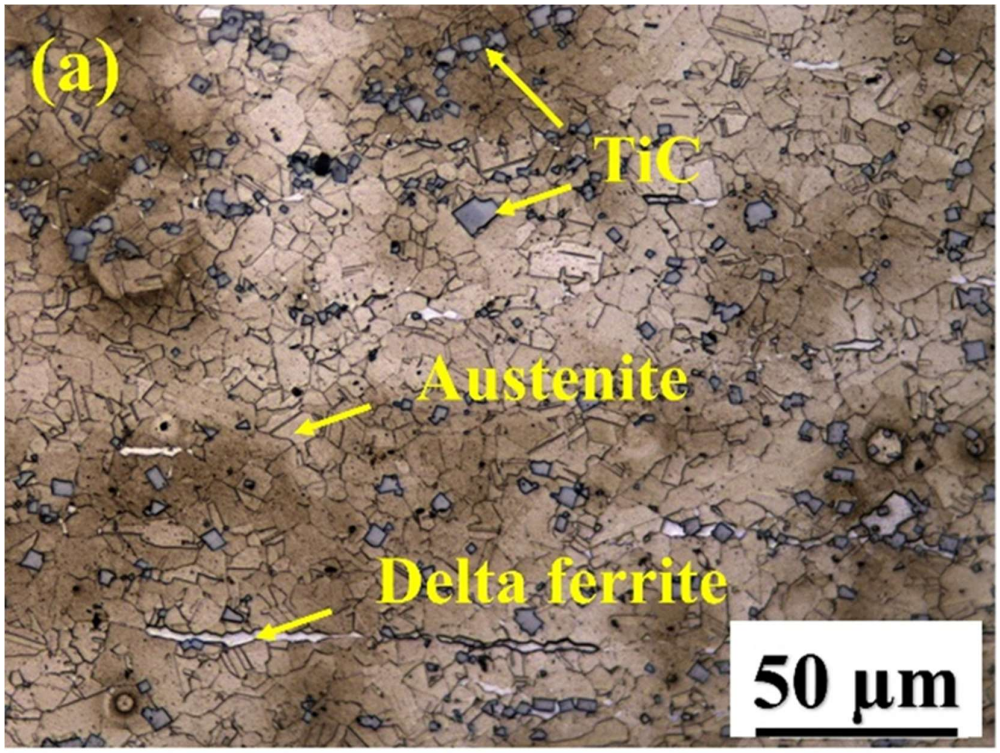
(a)
TiC
Austenite
Delta ferrite
50 µm

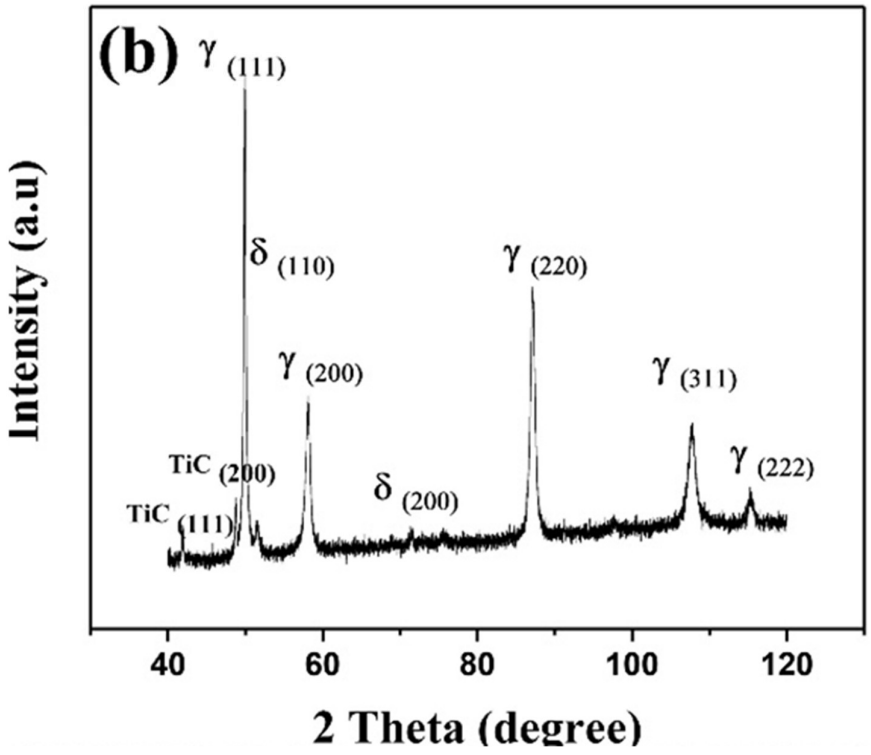
(b)
γ (111)
δ (110)
γ (220)
γ (200)
γ (311)
TiC (200)
γ (222)
δ (200)
TiC (111)
Intensity (a.u)
40
60
80
100
120
2 Theta (degree)

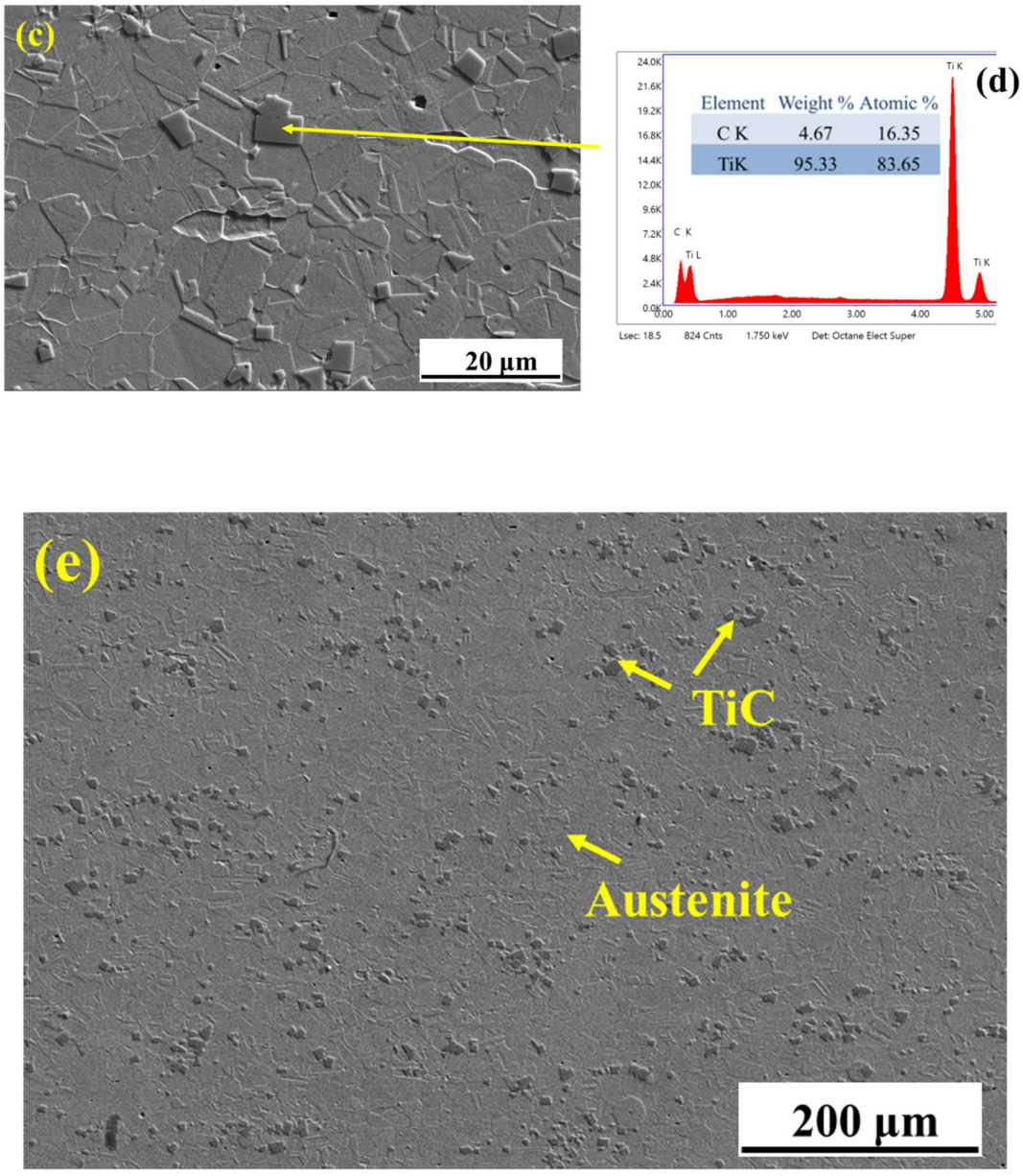
(c)
20 µm
(d)
Element Weight % Atomic %
C K 4.67 16.35
TiK 95.33 83.65
Ti K
C K
Ti L
Ti K
24.0K
21.6K
19.2K
16.8K
14.4K
12.0K
9.6K
7.2K
4.8K
2.4K
0.0K
0.00
1.00
2.00
3.00
4.00
5.00
Lsec: 18.5
824 Cnts
1.750 keV
Det: Octane Elect Super
(e)
TiC
Austenite
200 µm

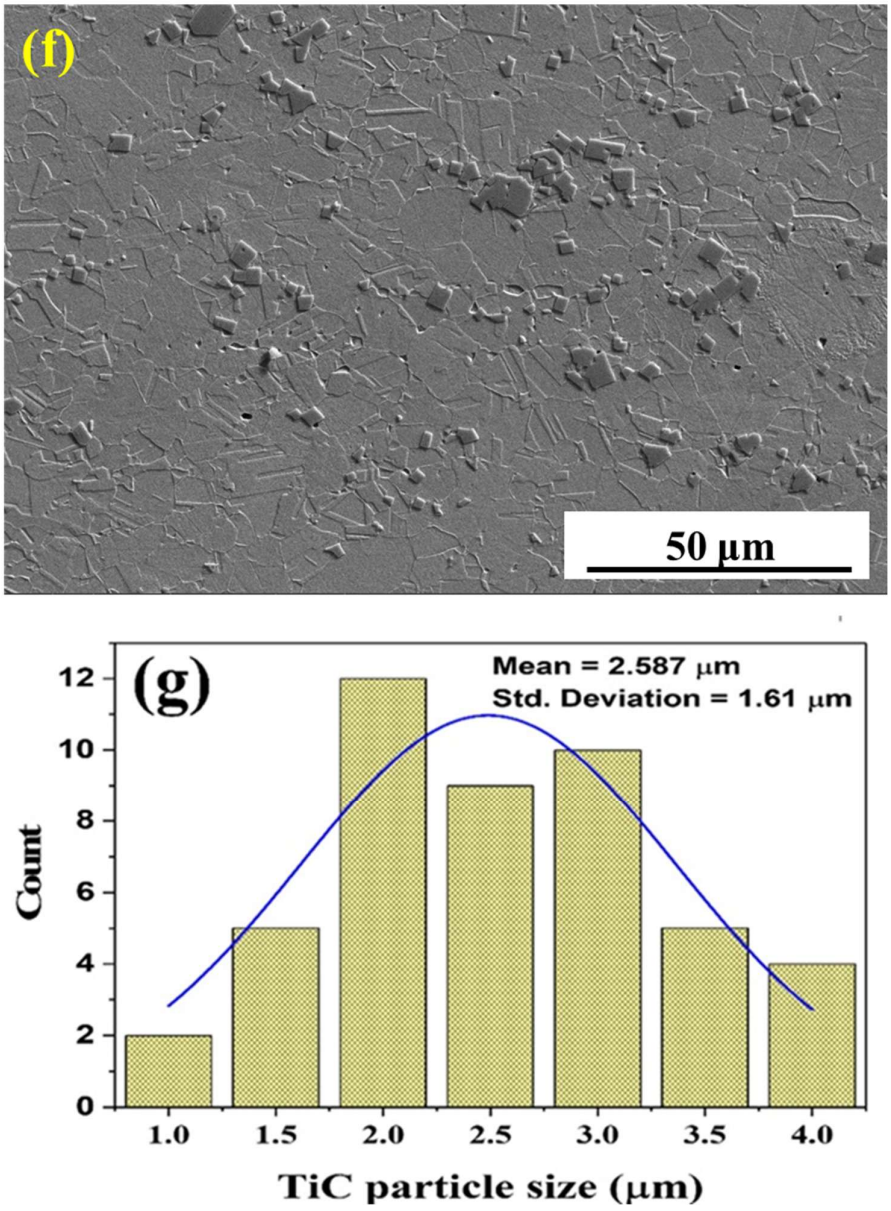

Figure 4.2: (a) Optical micrographs of PD2-S, (b) XRD pattern of PD2-S. SEM secondary electron micrograph of PD2-S (c) at 5000X showing TiC particles on which EDS spectrum is taken (d) EDS spectrum of TiC particle shown in Figure 4.2(c), (e) at 1000X showing TiC particle distribution (f) SEM secondary electron micrograph of PD2-S at 2500X and (g) TiC particle size distribution chart of Figure 4.2(f).

The image quality (IQ) map obtained from EBSD analysis (Figure 4.3(a)), reveals the austenite grains with distinct annealing twins within the microstructure. The white grains are austenite, and the black grains represent TiC particles. There is no delta ferrite in the image quality map of PD2-S. The XRD observation shows delta ferrite. This discrepancy compared to XRD in EBSD is due to the limited area covered in the EBSD scan. The grain size versus area fraction chart (shown in Figure 4.3(b)) reports the average grain size of austenite to be 6.48 ± 3.31 μm. Observations from both the optical micrograph and the grain size versus area fraction chart indicate some variation in grain size, likely due to the limited area covered in the EBSD scan.

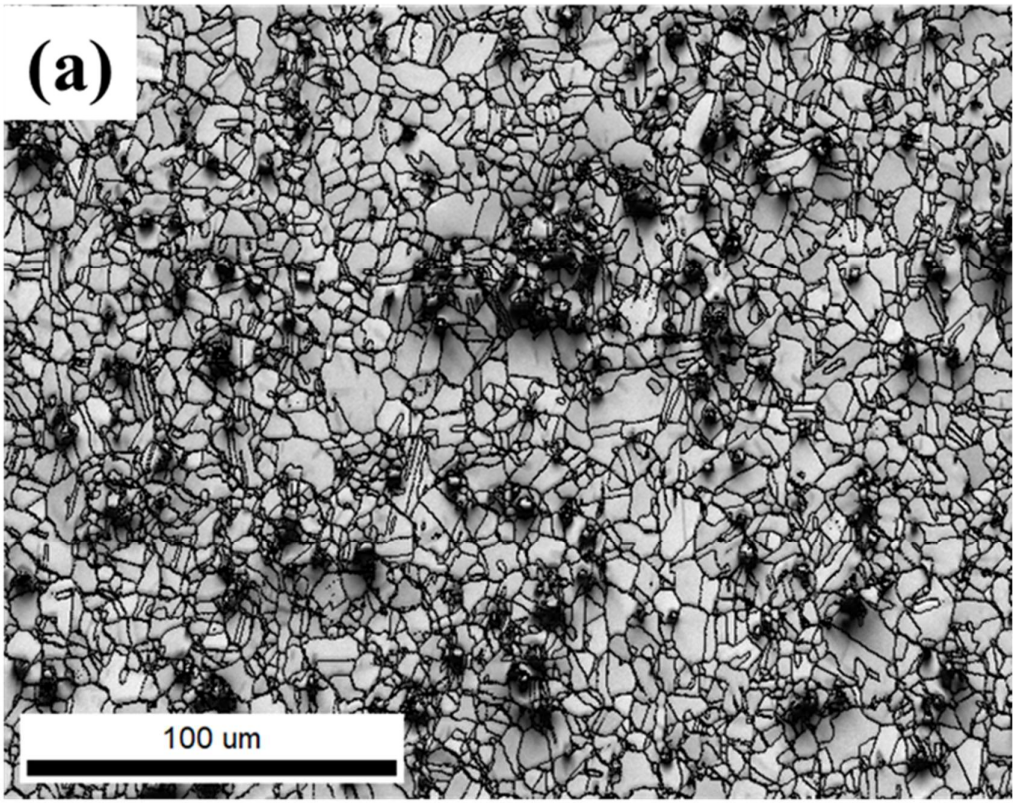

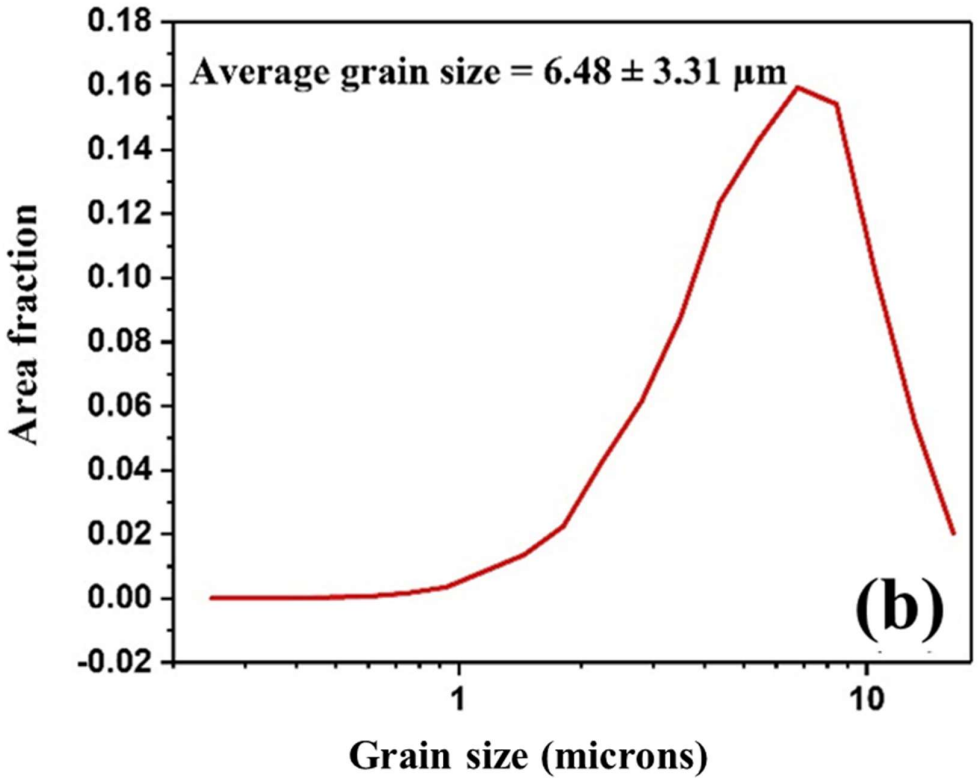

Figure 4.3: (a) IQ map, (b) grain size vs area fraction chart of PD2-S.

4.2.4 Tensile Properties

The engineering stress-plastic strain curve of PD2-S is shown in Figure 4.4(a). PD2-S exhibited a yield strength (YS) of 578 ± 9 MPa, an ultimate tensile strength (UTS) of 920 ± 13 MPa, and a plastic elongation (P.E.) of 35.3 ± 1.3 %. The UTS/YS ratio for PD2-S was calculated to be 1.59. SEM fractography of the tensile-tested PD2-S specimens (Figure 4.4(b)) reveals primarily dimpled features with an average size of 6.5 ± 1.7 µm, accompanied by tearing ridges, indicating a predominantly ductile fracture mode due to micro void coalescence.

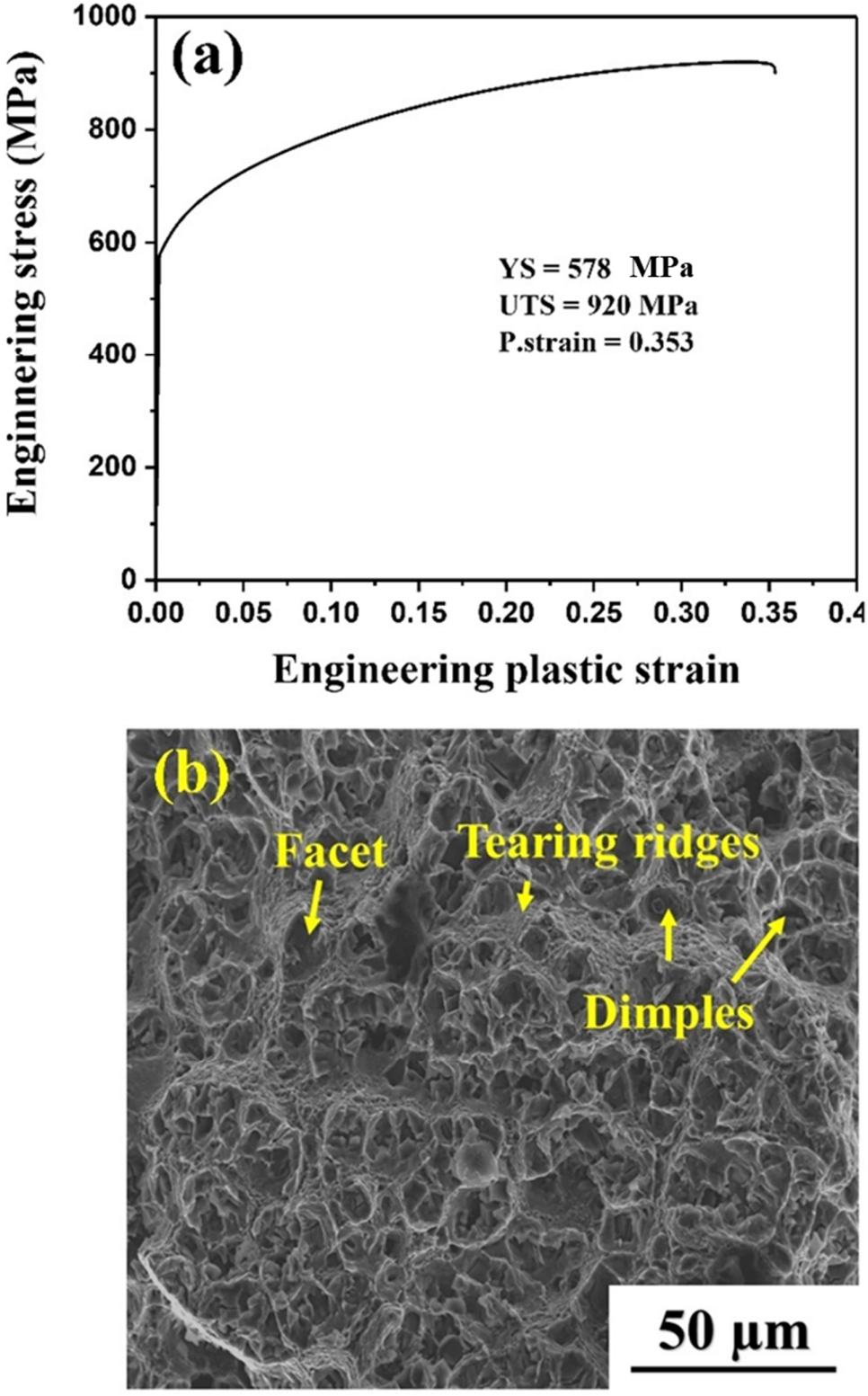

Figure 4.4: (a) Engineering stress- plastic strain curve of PD2-S and its (b) SEM secondary electron image of fracture surface.

4.3 Discussion

Results are explained in terms of Physical properties, Carbon content analysis, Microstructure, Strengthening Mechanisms and Work hardening behavior.

4.3.1 Physical properties

Austenitic steels have density of 8.15 g/cc and Young's Modulus of 195 GPa [20]. The addition of aluminum causes ~8.4% reduction in density for PD2-S. The presence of 4.5 % TiC decreases the density further by ~2.1% and remaining ~5% by high concentrations of C. The formation of TiC improves the elastic modulus of PD2-S by 7 GPa, due to higher modulus (400 GPa [66]) of reinforcement . Existing literature [11], [20], [129] suggests that the introduction of only 1 mass% of aluminum can result in a decrease in the elastic modulus of approximately 2-2.5%. As a consequence, it is anticipated that the elastic modulus of PD2-S experienced a decrease of around 13-16% because of 6.5% Al [11]. The measured elastic modulus value of PD2-S is 176 GPa which is 9.7% lesser than the conventional austenitic steels without aluminum[20].

4.3.2 Carbon content analysis

Analyzed PD2-S composition contains 1.15 mass % C. The overall density of the composite is 6.84 g/cc. The material contains 4.5 vol. % or 0.0324 mass percentage of TiC. TiC consists of 0.2007 mass percentage of carbon. Therefore, the amount of carbon tied up in TiC is 0.65 mass % C. As a result, the carbon in austenitic matrix in PD2-S is calculated to be 0.5 mass %.

To further confirm the carbon content within the austenite matrix of PD2-S, Chu et al. [12] correlated the lattice constant of austenite with mass % of alloying elements. This correlation is given by Equation 4.1.

$$a_0(\pm 0.0003) = (0.3570 \pm 0.0016) + (0.000065 \pm 0.000042)Mn + (0.00095 \pm 0.000071)Al + (0.0021 \pm 0.00052)C - (0.00101 \pm 0.00026)Si \quad [4.1]$$

Where, lattice constant (a_0) is in nm and Fe, Mn, Al, C are in mass %.

Based on the d-spacing values calculated from XRD data, the average lattice constant is calculated to be 0.36 nm. Substituting the mass percentages of Mn (21.75±0.16%) and Al (6.53±0.03%) obtained through SEM-EDS analysis in Equation 4.1, the mass % of carbon of austenite is found to be in the range of 0.52-0.56 mass %.

4.3.3 Microstructure

Phase fraction diagram of Fe-18Mn-6.5Al-1.15C-2.5Ti (PD2) calculated by using ThermoCalc predicts 94.2 % austenite, 1% delta ferrite and 4.8% TiC at homogenization temperature of 1080 °C. Hot rolling of the homogenized steel breaks the dendritic structure of austenite to granular structure and delta ferrite to elongated structure. On the other hand, cuboid type of TiC is observed. Due to the presence of second phases, the austenite grains are gets refined as these phases restricts the growth of austenite grains. By air cooling of hot rolled material, it is anticipated that some amount of kappa carbide precipitates forms in this material [20]. According to phase fraction diagram also, the formation of kappa carbides is observed. Due to the presence of 6.5% Al, the delta ferrite is expected to be stable at room temperature. Then solutionizing of air-cooled steel at 950 °C, dissolves kappa carbides but delta ferrite and TiC remains get unchanged. Solutionized structure of austenite, delta ferrite and TiC gets frozen by quenching in water. As a result, solutionized and quenched PD2-S steel consists of 92.5% fine austenite grains, 3% elongated delta ferrite and 4.5% rectangular type TiC. A small deviation between the experimental and predicted volume percentages is observed.

4.3.4 Strengthening mechanisms and its contribution to yield strength

The yield strength of the PD2-S steel is calculated based on applicable strengthening mechanisms with respect to their composition and amounts of phases.

The yield strength (σ_γ) of austenite in PD2-S is calculated using Equation 4.2 [50].

$$\sigma_\gamma = \sigma_P + \sigma_D + \sigma_{SS} + \sigma_{GB} \quad [4.2]$$

Where σ_P is Peierls stress, σ_D is dislocation strengthening, σ_{SS} is solid solution strengthening, and σ_{GB} is grain boundary strengthening, respectively. All the stress components are given in Table 4.2.

The Peierls stress σ_P is given by $3\tau_0$ [116],where τ_0 is shear stress which is $2*10^{-4}G$[117]. Here G is the shear modulus. Taking respective G value as 70 GPa for PD2-S, the Peierls stress is calculated as 42 MPa (Table 4.2).

σ_D is determined using Taylor expression as given in Equation 4.3 [118]

$$\sigma_D = M\alpha Gb\sqrt{\rho} \quad [4.3]$$

Here, M is the Taylor factor of austenite (3.1, calculated from EBSD data), $\alpha\ is$ Taylor constant (0.24) [119], b as Burger vector which is 2.6 Å for austenite. ρ is the dislocation density which is calculated using Equation 4.4 [130].

$$\rho = 14.4(\frac{\epsilon^2}{b^2}) \quad [4.4]$$

Where ε is the micro strain. Taking ε as 0.00071 for PD2-S (calculated from XRD data by Williamson-Hall equation), the calculated σ_D is found to be 114 MPa (Table 4.2).

σ_{SS} is estimated by using the Equation 4.5 [120].

$$\sigma_{SS} = 279 * wt.\%C - 1.5 * wt.\%Mn + 20.5 * wt.\%\ Al \quad [4.5]$$

The estimated σ_{SS} for PD2-S is 241 MPa (Table 4.2).

The grain boundary contribution to yield strength (σ_{GB}) is calculated using Hall-Petch relation and is given by Equation 4.6 [121].

$$\sigma_{GB} = K_B . d^{-1/2} \quad [4.6]$$

where K_B is grain boundary locking parameter, which is taken as 330 MPaμm$^{1/2}$ for similar low-density steel [78] and d is grain size of austenite which is 10 μm for PD2-S. The estimated σ_{GB} value for PD2-S is 134.7 MPa (Table 4.2). Therefore, the yield strength (σ_γ) of austenite in PD2-S is calculated to be 532 MPa.

PD2-S contains additional 4.5 vol % of incoherent TiC precipitates. The contribution of TiC precipitates(σ_{Pr}) to yield strength is calculated using Equation 4.7 given by Ashby-Orowan [120].

$$\sigma_{Pr} = 0.538Gb(\frac{f^{\frac{1}{2}}}{D})\ln(\frac{D}{2b}) \quad [4.7]$$

where f is the volume fraction (0.045), D is the diameter of the particles (2.59 μm). The estimated σ_{Pr} is 4.64 MPa (Table 4.2). Thus, the estimated yield strength of PD2-S is 537 MPa, which is 41 MPa lower than the measured yield strength of 578 MPa. This discrepancy is possibly due to neglecting the contribution from 3 vol % of delta ferrite. Strength of delta ferrite could not be calculated due to shortage of composition and strength data. Solid solution strengthening is the primary mechanism for strengthening due to the presence of higher amounts of alloying elements followed by grain boundary and dislocation.

Table 4.2: Contribution of strengthening mechanisms to yield strength of PD2-S.

Strengthening mechanism	σ_P	σ_{SS}	σ_D	σ_{GB}	σ_{Pr}	Calculated YS	Experimental YS
Contribution to YS (MPa)	42	241	114	134.7	4.6	536.3	578

4.3.5 Work hardening behavior

The experimental logarithmic true stress versus logarithmic true plastic strain plot of PD2-S fitted with plots made through Hollomon [109], Ludwik [110], Ludwigson [112], Swift [111], and Voce[113] flow models, which are displayed in Figure 4.5 (a). The slopes or work hardening rates undergo two types of changes: one at low strain, and another at high strain, with a transition occurring at intermediate strain. Out of the considered models, the Ludwigson relationship was found to be the best fit for the experimental data. This is supported by the highest R^2 (coefficient of determination) values and the lowest ξ^2 (sum of squares of deviation of calculated stress values from experimental stress values) values of 0.9998 and 3.96 MPa, respectively.

Ludwigson flow behavior is given by Equation 4.8.

$$\sigma = exp(K_1 + n_1\varepsilon) + K\varepsilon^n \quad [4.8]$$

Where K_1 and K are strength coefficients and n_1, and n are work-hardening exponents, respectively, at low and high strain regimes [122].

The strength coefficient ($\exp(K_1)$) of PD2-S in low-strain regimes is 556 MPa (Table 4.2). The corresponding work-hardening exponent (n_1) is 0.35. In high strain regimes, PD2-S exhibits a strength coefficient (K) value of 1381 MPa and work hardening exponent (n) value of 0.65. The differentiation of the Ludwigson equation with respect to strain yields Equation 4.9, which quantifies the variations in the work hardening rate.

$$\frac{d\sigma}{d\varepsilon} = n_1 \exp(K_1 + n_1\varepsilon) + Kn\varepsilon^{n-1} \quad [4.9]$$

Equation 4.9 indicates the existence of two distinct variations in work hardening rate relative to true strain.

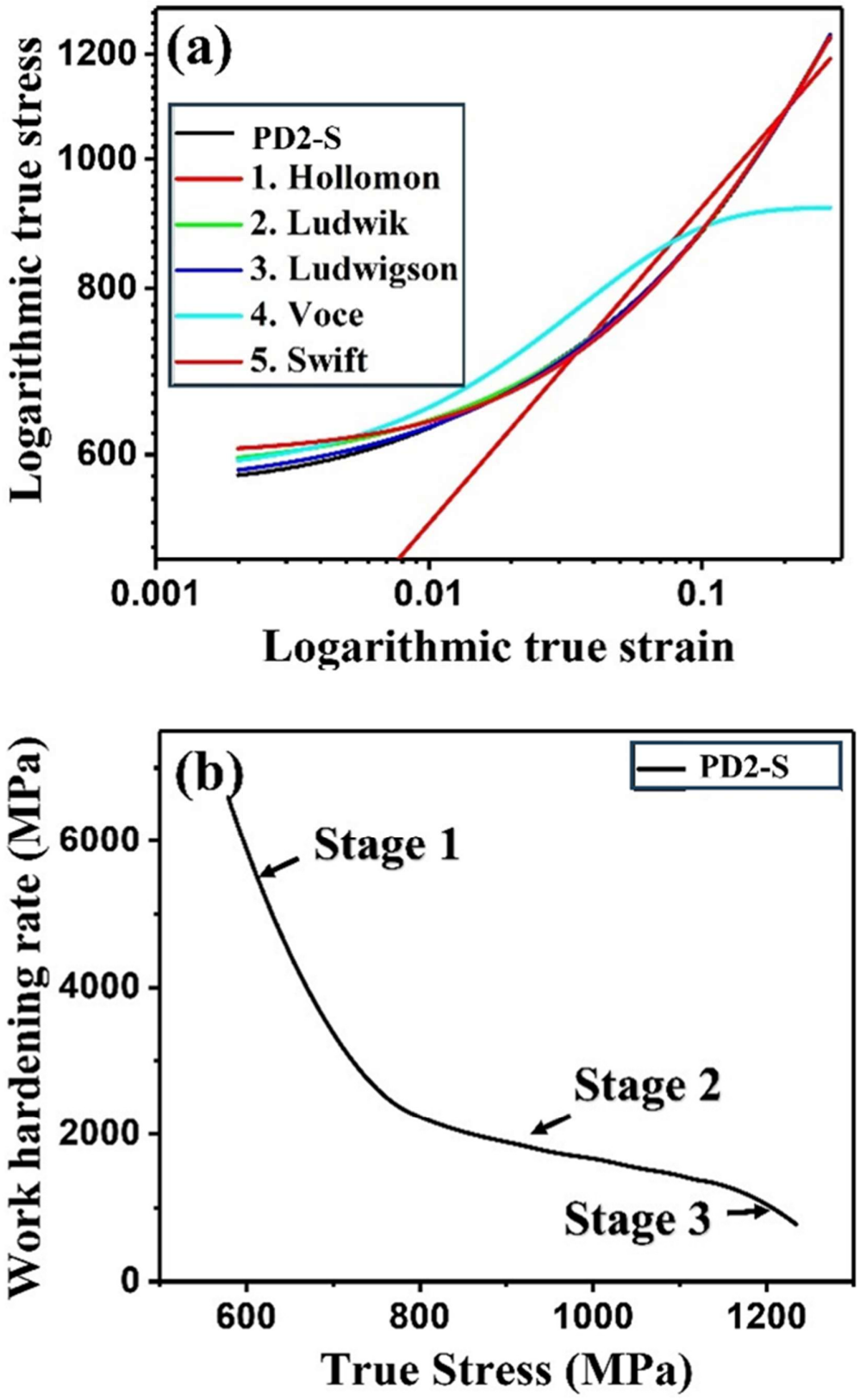

Figure 4.5: (a) Logarithmic true stress vs. logarithmic true plastic strain plots of PD2-S fitted with various models, (b) Work hardening rate vs true plastic stress diagram.

Table 4.3: Strength coefficients, work-hardening exponents and fitting parameters with Ludwigson flow equation for PD2-S.

Steel	exp(K_1) (MPa)	n_1	K (MPa)	n	R^2	χ^2
PD2-S	556	0.35	1381	0.65	0.9998	3.96

The experimental work hardening rate variation in relation to true plastic stress for PD2-S during three stages (Stage 1-Stage 3) is depicted in Figure 4.5(b). The initial stage demonstrates a pronounced decline in the work hardening rate. In Stage 2, constant decrease in slope is observed. Stage 3 is characterized by a dynamic recovery.

At a low-stress regime, the work hardening rate decreases rapidly with gradients of -22 MPa for PD2-S (approximately 550-750 MPa). It is also referred to as the easy glide stage, primarily occurs due to the planar flow of dislocations (Planar slip) over long distances, where the motion of dislocations is hindered by minimal obstacles like precipitates or grain boundaries [123]. The rate of accumulation of dislocations is negligible in this stage.

At higher strain regimes, the work hardening rate of PD2-S (750-1150 MPa) decreases gradually. The gradients of the work hardening rate of PD2-S with respect to true stress is -2.55. The activation of cross-slip and multiple-slip systems enhances the formation of heterogeneous dislocation structures comprising dislocation tangles, walls, and cells. The proportion of these structures increases as the plastic strain during stage 2 progresses [125]. Stage 2 corresponds to the phase of enhanced dislocation storage, characterized by the proliferation of wall and cell structures, resulting in an increase in dislocation density.

Stage 3 represents the dynamic recovery phase, wherein dislocations undergo annihilation, leading to a reduction in the work hardening rate. The linear relationship observed between the hardening rate ($\frac{d\sigma}{d\epsilon_p}$) and true plastic stress (σ) curves in the third stage (Figure 4.6)

can be most effectively elucidated similar to the Kock, Mecking, (KM) dislocation models : [118], [126], as expressed in Equation 4.10.

$$\frac{d\sigma}{d\epsilon} = \theta_0 + m\sigma \quad [4.10]$$

Here, $\frac{d\sigma}{d\epsilon}$ and σ represent the strain hardening rate and the true stress, respectively. The initial work-hardening rate, denoted as θ_0, signifies the athermal mobility of dislocation storage that has been arrested following a proportional travel distance relative to the average slip spacing. The term m correspondingly refers to the gradient of the linear regimes attributed to the elimination of dislocations caused by cross slip during dynamic recovery [127]. A high value of θ_0 indicates a high dislocation storage capacity signifying the material's ability to retain dislocations. Conversely, a high negative value of m suggests high dynamic recovery implying that the material experiences work softening.

The results of the linear fitting for the third stage of both PD1-S and PD2-S are depicted in Figure 4.6. The Adjusted R^2 value of the fitted curves approaches 1, indicating a strong correlation between the experimental data and the fitted curve. The dislocation storage capacity (θ_0) of PD2-S is determined to be 9162 MPa. Conversely, the negative slope (m) of the curve for PD2-S is 7 GPa. The presence of TiC precipitates may account for the lower dynamic recovery in PD2-S.

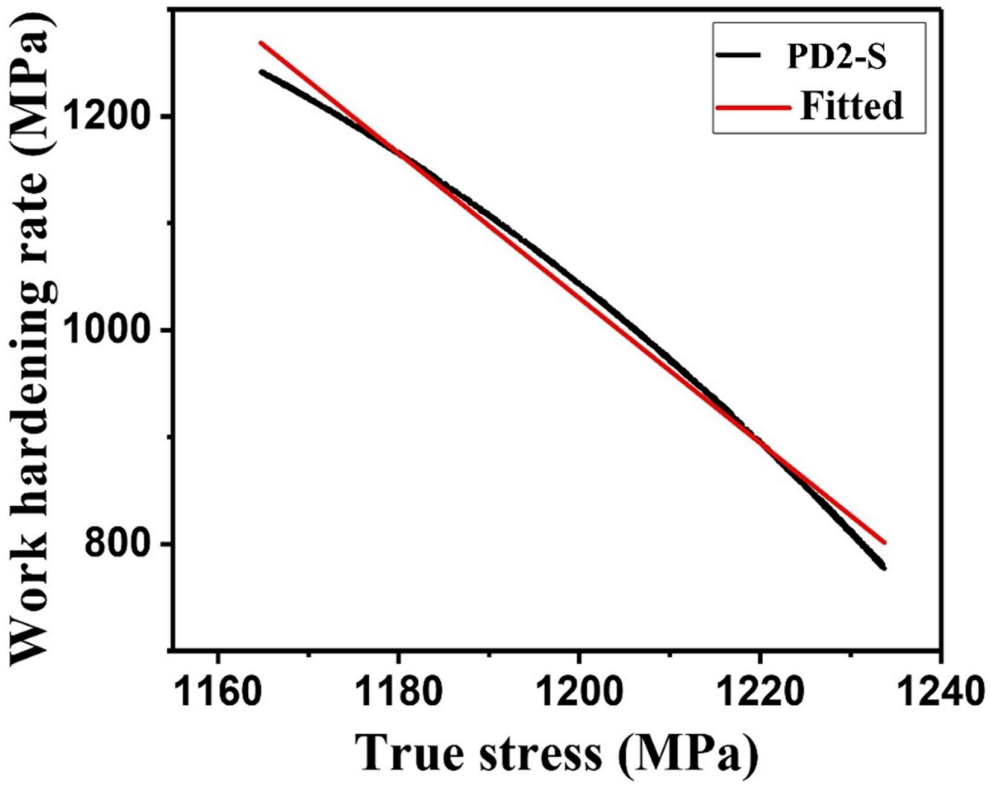

Figure 4.6: Linear fitting curves of the third stage in PD2-S using Kock, Mecking, (KM) based dislocation models.

PD2-S exhibited lower elongation due to the presence of brittle TiC precipitates. The presence of cleavage facets further confirms that PD2-S failed in a mixed mode of ductile-brittle fracture.

It is predicted that the performance and weight savings of Fe-Mn-Al-C low-density steels for automotive applications would be enhanced by combining high strength, low-density, and a high elastic modulus. Therefore, Ti and extra amount of C is intentionally added to get in-situ TiC in the steel to increase its strength and elastic modulus, while slightly reducing the density, in order to achieve a better combination of properties. The present steel is being developed as one of the third-generation advanced high strength steel (AHSS). The tensile strength of this group of steels ranges from 500 MPa to 1700 MPa,

with total elongation in the range of 58% to 12% [131]. The tensile properties of PD2-S satisfy the requirements with the added advantage of 12% reduced density/mass.

4.4 Conclusions

Investigation on in-situ formation of TiC in an austenitic low-density steel brings the following conclusions.

- X-ray diffraction analysis confirms the presence of 4.5 vol% titanium carbide (TiC) in the microstructure, which is formed through an in-situ reaction process during casting.
- The presence TiC greatly reduces the grain size to 10 μm.
- By incorporating TiC, a significant increase in elastic modulus of 7 GPa and a further decrease in density of 2.1% are achieved.
- The austenitic low-density steel is strengthened mainly by solid solution followed by dislocation and grain boundary strengthening. In-situ TiC formation enhances grain boundary, and dislocation strengthening significantly though contribution of precipitation strengthening is marginal due to coarse size.
- PD2-S follows the Ludwigson flow behavior, characterized by the presence of two distinct slopes of easy glide and cross slip, respectively.